

# RSC Advances



This is an *Accepted Manuscript*, which has been through the Royal Society of Chemistry peer review process and has been accepted for publication.

*Accepted Manuscripts* are published online shortly after acceptance, before technical editing, formatting and proof reading. Using this free service, authors can make their results available to the community, in citable form, before we publish the edited article. This *Accepted Manuscript* will be replaced by the edited, formatted and paginated article as soon as this is available.

You can find more information about *Accepted Manuscripts* in the [Information for Authors](#).

Please note that technical editing may introduce minor changes to the text and/or graphics, which may alter content. The journal's standard [Terms & Conditions](#) and the [Ethical guidelines](#) still apply. In no event shall the Royal Society of Chemistry be held responsible for any errors or omissions in this *Accepted Manuscript* or any consequences arising from the use of any information it contains.

Cite this: DOI: 10.1039/c0xx00000x

www.rsc.org/xxxxxx

ARTICLE TYPE

# Surface characteristics, corrosion resistance and MG63 osteoblast-like cells attachment behaviour of nano SiO<sub>2</sub>-ZrO<sub>2</sub> coated 316L stainless steel

Arthanari Srinivasan, Nallaiyan Rajendran\*

Received (in XXX, XXX) Xth XXXXXXXXXX 20XX, Accepted Xth XXXXXXXXXX 20XX

DOI: 10.1039/b000000x

Nano SiO<sub>2</sub> (NS), ZrO<sub>2</sub> (NZ) and SiO<sub>2</sub>-ZrO<sub>2</sub> (NSZ) mixed oxide coatings on to 316L stainless steel (SS) were developed by simple sol-gel technique with varying Si:Zr ratios (100:0, 70:30, 50:50 and 0:100). Surface characteristics, corrosion resistance and the initial cell attachment behaviour of MG63 osteoblast are studied. The formation of NSZ mixed oxide was ensured from the shift in Si-O-Si<sub>asym</sub> band to lower wave number with increasing Zr content in attenuated total reflectance infra-red (ATR-IR) spectra. X-ray diffraction studies also further confirmed the formation of mixed oxides. The formation of spherical particle with nanometre scale was confirmed from scanning electron microscopy (SEM) images and the particle size reduced as the Zr content is increased. The simulated body fluid (SBF) contact angle values of NS, NSZ-73 and NSZ-55 were reduced to about three and two times compared to NZ and uncoated 316L SS respectively. Potentiodynamic polarization studies revealed the lower corrosion current density (*i*<sub>corr</sub>) values for all the coated 316L SS. In particular, NSZ coatings exhibited significant reduction in *i*<sub>corr</sub> values, further confirming that the addition of Zr to NS improved their corrosion resistance in SBF solution. The initial attachment of MG 63 osteoblast-like cells on uncoated and coated 316L SS was studied using fluorescent microscopy by nuclei and actin protein staining. The results showed that the cell attachments were good for NS, NSZ-73 and NSZ-55 with the development of Actin stress fibres with flattened cell morphology. However, the cell attachment was not significant for NZ. The variation in cell attachment behaviour is attributed to the surface characteristics and hydrophilic/hydrophobic nature of the coatings.

## 1. Introduction

Development of 316L SS as metallic implant materials is one of the key areas in biomaterials research for orthopaedic implants without any adverse effects.<sup>1-3</sup> Some of the major issues viz., bioactivity, corrosion resistance to the physiological environment etc., need to be addressed when the implant is in service.<sup>4,5</sup> Materials satisfying the above characteristics could act as suitable candidates for implant applications. However, often an implant material fails in fulfilling both the characteristics.<sup>6</sup> New alloys are developed by introducing several alloying elements with optimum concentrations, which make the materials suitable for practical applications.<sup>7</sup> However, altering the alloy composition mainly focuses on improving the mechanical properties and corrosion resistance of the alloys. Hence, it is essential to modify the surface, which could persuade the implant materials to be bio active.

Surface modification of implant materials with porous bio-inert/ bioactive ceramic materials has become one of the thrust areas in recent research scenario.<sup>8-10</sup> These porous ceramic coatings generally improve the bioactivity and corrosion resistance as well to some extent. There are several porous

ceramic materials viz., Ca<sub>3</sub>(PO<sub>4</sub>)<sub>2</sub>, TiO<sub>2</sub>, ZrO<sub>2</sub>, Nb<sub>2</sub>O<sub>5</sub>, glass ceramics etc., widely used to modify the surface of implant materials.<sup>11-17</sup> Coating comprising of porous Ca<sub>3</sub>(PO<sub>4</sub>)<sub>2</sub> and TiO<sub>2</sub> found to improve the bioactivity rather than corrosion resistance. Coating of 316L SS surface with bioactive bone like hydroxyapatite (HAp) contributes to the improvement of bioactivity.<sup>18</sup>

Interaction of biological cells with these micro/nano textured ceramic coated surfaces needs to be investigated and it not only helps in understanding but also in selecting materials with suitable surface characteristics for implant applications. Several reports are available on cell attachment and proliferation on implant surfaces. Osteoblast responses on to ceramic coatings with varying surface characteristics have been studied in detail.<sup>19</sup> They have report that the SiO<sub>2</sub>-TiO<sub>2</sub> coating exhibited higher cell proliferation rate and the chemical composition significantly affected the cell responses. Takahiro et al.<sup>20</sup> reported the significance of surface chemistry viz., hydrophilicity/hydrophobicity and surface roughness on the cell adhesion behaviour on implant material. According to them the surface hydrophilicity improved the cell adhesion and proliferation

immediately after seeding. In addition to that, the protein adsorption was also higher for hydrophilic surfaces than hydrophobic surfaces. In order to have better cell adhesion, a constant contact is required between the cells and surface.

Hydrophobic surfaces fail to establish the constant contact with cells. Silica based organic-inorganic hybrid coatings have also been investigated for biomedical applications to improve the corrosion resistance of 316L SS in Ringer's solution. In vitro cytotoxicity study using L929 cells revealed that the cell morphology was found to be same both in uncoated and coated substrates.<sup>21</sup>

Cell proliferation of human dermal fibroblasts (HDFn) over TiO<sub>2</sub>-ZrO<sub>2</sub> coated 316L SS was found to be effective compared to uncoated 316L SS.<sup>22</sup> Surface topography of hydroxyapatite (HAp) is also found to influence the osteoblast attachment. Cell attachment and differentiation were higher for more complex and micro rough surfaces compared to smooth surfaces.<sup>23</sup> Hence, it is clear that the study of surface characteristics on the corrosion behaviour and initial cell attachment behaviour is important to develop the materials without any adverse effect. Therefore, in the present investigation, NS, NZ and NSZ coatings were produced onto 316L SS by simple sol-gel technique to systematically study the phase structure, morphology, topography, wettability, corrosion behaviour and initial MG 63 osteoblast-like cell attachment. The formation of coating and the effect of surface characteristics on the initial cell attachment behaviour have been discussed.

## 2. Experimental

### 2.1 Preparation of NS, NZ and NSZ sol

NS, NZ and NSZ sols were prepared by simple sol-gel techniques at ambient temperature. Tetraethyl orthosilicate (TEOS) and Zirconium (IV) isopropoxide (Sigma Aldrich, USA) were used as precursor materials in as received condition for Si and Zr respectively. The reaction was initiated by adding calculated amount of precursor materials into ethanol (Jiangsu Huaxi International Trade Co. Ltd., China) during stirring at ambient temperature. The composition of precursor materials is given in Table 1. Initially, the sol was transparent and after the addition of water, it turned into a white turbid sol. NaOH was then added to the reaction mixture as a self-template etching base catalyst during stirring and continued for 12 h at about 1500 rpm. The same procedure was adopted for the preparation of mixed NSZ with the only variation in precursor ratio.

### 2.2 Development of NS, NZ and NSZ coatings

The coatings were produced onto 316L SS by dip coating technique. Initially the commercially available 316L SS samples (25 mm x 15 mm x 2 mm) were ground with 120# silicon carbide (SiC) emery sheet to remove native oxides, contaminant present on the surface and to have rough surface, which could improve the adhesion of ceramic coatings. The ground samples were ultrasonicated in acetone: ethanol (1:1) mixture for 15 min., then thoroughly rinsed with double distilled water and air-dried. In order to produce the coatings, the samples were dipped into the sols taken in a 10 ml glass beaker, allowed for 100 s as waiting time, and withdrawn at a speed of 5 cm/min. The coated samples were cured at room temperature for 12 h and stored in desiccators

for further characterizations.

### 2.3 Characterization of NS, NZ and NSZ coatings

#### 2.3.1 Surface and phase composition

ATR-IR spectroscopic studies of coated specimens were carried out using Perkin Elmer UATR Spectrum Two Spectrometer, Singapore. X-ray diffraction studies were carried out using Pan Analytical Xpert-pro diffractometer using Cu K $\alpha$  radiation, with 40 KV and 30 mA, at a scan rate of 2°/min. Surface morphology of coated samples were observed using JEOL (JSM-6490 L) analytical scanning electron microscope (SEM) with energy dispersive X-ray analysis (EDAX) with acceleration voltage of 10 kV. The coated samples were mount into cold setting acrylic powder and ground up to 1500 # SiC emery sheets and subsequently polished to 0.05  $\mu$ m alumina powders to obtain fine finished surfaces. The cross-sectional morphology of all these coated samples was observed using SEM to measure coating thickness. Surface topography and average roughness of the specimens were obtained using XE-70 model Atomic Force Microscope (AFM), Park systems, Korea. AFM images were taken in non-contact mode with SiC cantilever. Particle size of the prepared ceramic materials was analyzed by dispersing the as prepared ceramic powders (1 mg/10 ml) in Milli-Q water and measured using Malvern Zetasizer version 7.01 instruments. Simulated body fluid (SBF, composition is given in Table 2)<sup>24</sup> contact angle values of the uncoated and coated samples were measured using inbuilt optical microscope attached with CCD camera.

#### 2.3.2 Adhesion measurements

Adhesion of the produced coatings was evaluated using Elcometer 107 Cross Hatch Cutter according to ASTM D3359-B<sup>25</sup> and the detailed experimental procedure is mentioned elsewhere.<sup>26</sup> The adopted experimental procedure is explained here. In order to measure the coatings adhesion, initially two cuts were made over the coated surface at right angle to each other and it resulted in a grid of small squares. Then, the surface was gently wiped using brush to remove detached flakes. Adhesive tape was then placed over the surface and ensured good adhesion between the tape and the coating. After about 60 sec., the tape was removed by pulling in a single smooth action at an angle of 180° to the coating surface. After removal of the tape the adhesion was assessed by viewing the lattice of cuts using an illuminated magnifier and the grid of squares were compared against ASTM standard.

#### 2.3.3 Electrochemical corrosion behaviour

Electrochemical corrosion behavior of uncoated and all the coated specimens were tested in SBF solution at 37 °C using conventional three-electrode cell. CH Instruments 700 series Electrochemical Workstation, USA was used to carry out the corrosion experiments. Coated specimens with an exposed area of 1 cm<sup>2</sup> were used as working electrode (WE). Pt sheet and saturated calomel electrode (SCE) were used as counter (CE) and reference electrodes (RE) respectively. Potentiodynamic polarization study was carried out after stabilizing the open circuit potential (OCP) for about 30 min. in the potential range of -0.250 V + OCP to 1.0 V<sub>SCE</sub> at a scan rate of 1 mV/s. The obtained results are represented as Potential vs. Log i plots. Tafel

extrapolation method was used to extract the polarization parameters from the obtained results.

### 2.3.4 Cell attachment studies

The ethylene oxide (EtO) sterilized samples for cell attachment were placed in a 24 well plate and incubated in culture medium for 1 h at 37°C in a humidified incubator. After the incubation, the culture medium was removed and MG-63 osteoblast-like cells were seeded drop wise onto the top of the samples ( $1 \times 10^5$  cells/sample) and incubated at 37°C for 24 h. After 4 h, the samples were fed with additional serum containing medium. After 24 h of incubation, the samples were washed with phosphate buffered solution (PBS), fixed with 4% paraformaldehyde for 15 min. and permeabilized with 0.5% Triton X-100 (in PBS) for exactly 5 mins. The samples were then blocked using 1% fetal bovine serum (FBS) in PBS, washed, stained with 50  $\mu$ l of actin (in PBS) and incubated in dark for 1 h. The samples were then washed and stained with 50  $\mu$ l of 6-Diamidino-2-Phenylindolehydrochloride hydrate (DAPI) (in PBS) to stain the cell nuclei and incubated in dark for 5 min. DAPI bonds<sup>18</sup> with natural double-stranded DNA forming fluorescent complexes showing specific activity of proteins. Fixing and staining of all the samples with cells were carried out in silicone wells until the staining procedure gets completed. The samples were thoroughly washed and viewed under fluorescent microscope (Olympus-BX-51).

## 3. Results and Discussion

### 3.1 Attenuated total reflectance-infra red (ATR-IR) spectroscopy studies

ATR-IR spectra of NS, NZ, NSZ-73 and NSZ-55 coated 316L SS are given in Fig. 1. From the spectra of NS, it is seen that the peak appearing around 1073  $\text{cm}^{-1}$  was attributed to asymmetric stretching of Si-O-Si, and the corresponding bending vibration appeared at about 500  $\text{cm}^{-1}$ . Presence of peaks at about 800  $\text{cm}^{-1}$  and 950  $\text{cm}^{-1}$  were assigned to Si-O-Si<sub>bridge</sub> vibration and terminal -Si-OH stretching vibrations respectively.<sup>27</sup> In the case of NZ the band appearing at 1350-1400  $\text{cm}^{-1}$  was attributed to the deformation vibration of -Zr-OH.<sup>28</sup> The Zr-O and Zr-O-Zr bands were detected as weak signals at 583  $\text{cm}^{-1}$  and 506  $\text{cm}^{-1}$  respectively.<sup>29</sup> The formation of NSZ-73 and NSZ-55 were also confirmed from the shift in absorption bands towards low frequency. Si-O-Si<sub>asy</sub> of NSZ-73 and NSZ-55 were shifted from 1073  $\text{cm}^{-1}$  to 1060 and 1048  $\text{cm}^{-1}$  respectively. Further the Si-O-Si<sub>def</sub> band was also shifted to 455  $\text{cm}^{-1}$  and 442  $\text{cm}^{-1}$  from 462  $\text{cm}^{-1}$ . These results confirmed the formation of mixed SiO<sub>2</sub>-ZrO<sub>2</sub> coating. The shift in Si-O-Si<sub>bridge</sub> to lower wave number further confirmed the formation of Si-O-Zr<sub>bridge</sub>.

### 3.2 X-Ray diffraction (XRD) studies

The prepared coatings were analysed for their phase structure using XRD and the obtained patterns are given in Fig. 2. The broad peak appearing at 2 $\theta$  value of 20-30° centred at 23° for NS indicated the formation of SiO<sub>2</sub> with amorphous phase.<sup>27, 30</sup> In the case of NZ, the peak was observed between 25-35°, centered at 30° with slightly broad peak area and attributed to the formation of nano-crystalline ZrO<sub>2</sub>. XRD patterns of NSZ-73 and NSZ-55 were also found to be broader with shift in peak position

to higher 2 $\theta$  value with increasing Zr content, indicating the incorporation of Zr into the Si-O-Si matrix. Increasing Zr content also led to the broadening of peak, confirming reduction in particle size. However the peak was positioned between 2 $\theta$  values of NS and NZ, thus confirming the formation of mixed SiO<sub>2</sub>-ZrO<sub>2</sub> (NSZ). The peaks that appeared at 2 $\theta$  values of 74.68, 50.76 and 43.56 correspond to the planes (220), (200) and (111) of austenitic stainless steel.<sup>31</sup>

### 3.3 Surface morphological and cross-sectional studies

#### 3.3.1 Scanning electron microscopy and energy dispersive X-ray analysis (SEM- EDAX)

SEM images of NS, NZ, NSZ-73 and NSZ-55 coated 316L SS are shown in Fig. 3 (a-h). SEM images with higher magnifications are also included in the figure in order to clearly distinguish the coating morphology. It is seen from the micrographs that the NS exhibited spherical morphology and spread over the surface. However, the complete surface coverage was not ensured and this could be due to the formation of isolated spherical particles during the preparation of sol. SEM image of NZ with low magnification showed that the sample was completely covered by coating with micro cracks due to the smaller particle size. In order to verify the same, the particle size of the prepared ceramic materials were measured using particle size analyser and the obtained average particle sizes for NS, NZ, NSZ-73 and NSZ-55 have been compared and given in Fig. 3(i). From the figure it is seen that, the average particle size of NZ (~270 nm) was less when compared to NS (~530 nm). These results further substantiated the complete surface coverage by NZ coating. SEM images of mixed NSZ-73 and NSZ-55 coatings are given in Fig. 3 (e-h). From the SEM images it is seen that increasing Zr content in the coating produced more compact layer with significant reduction in micro cracks. The cracks are almost invisible in the case of NSZ-55, confirming the formation of compact layer over 316L SS and it could be due to the reduction in particle size with increasing Zr content (Fig. 3i). Energy dispersive X- ray analysis (EDAX) of all the coatings was carried out to confirm the composition of the coating and is also given in Fig. 3. A comparative plot of weight percentage obtained by EDAX for all the ceramic coatings are represented in Fig. 3 j for simple understanding. From the EDAX spectra of the coated samples, it is seen that the amount of alloying element content decreased, which is due to the existence of the coating over the surface. However, the amount of Fe was found to be high in the case of NS, as a result of incomplete surface coverage. The amount of Fe was found to be less with NSZ coated 316L SS.

Average coating thickness was measured for the produced coatings from the cross-sectional SEM images and shown in Fig. 4. It is seen from the figure that, among all the coatings, NS had relatively thick (~11  $\mu$ m) coating along with micro cracks across the coating. The existence of cracks could be attributed to the dehydration of water molecules during drying. NZ exhibited relatively compact coating with the thickness of about 6  $\mu$ m. The coatings thickness was found to be about 8  $\mu$ m for NSZ-73 and NSZ-55 coatings. All the coatings had relatively good contact with the substrate further confirming the formation of adherent coatings.

### 3.3.2 Atomic force microscopy (AFM) studies

AFM topographs of uncoated and all the coated samples are shown in Fig. 5 (a-e). Line scan was also carried out across the samples and are included in the figure. The AFM images were taken in non-contact mode with  $2.5 \times 2.5 \mu\text{m}$  area using SiC cantilever. Uniform grooves were observed for the uncoated samples, which are formed due to grinding of the samples before coating. The grooves were significantly minimized in the case of coated samples indicating that the coatings covered the ground surface. In addition to that, the spherical morphology was ensured for NS coating and uniformly distributed over the surface. It is interesting to note that, the particle size of NZ (Fig. 5c) was reduced without much alteration in the spherical morphology (Fig. 5c inset). The coating was also found to be relatively smooth with micro cracks for NZ. However, NSZ-73 and NSZ-55 exhibited similar topographical features and the coatings were found to be relatively rough and with increase in the amount of Zr. The existence of rough morphology could be due to the aggregation of ceramic particles over the surface.

Surface modification of implant materials is generally carried out to enhance the interaction between the biological medium with the implant material. One of the important factors which decide the interaction of cells is surface topography of the material.<sup>23, 32</sup> Roughness values of all the samples were measured by line scanning across the samples and the corresponding line profiles, histograms are also included in Fig. 5. The obtained  $R_a$  roughness values of uncoated and coated samples have been compared and are given in Fig. 6. From the figure it is seen that the  $R_a$  roughness value of NS was found to be about 26 nm where as in the case of NZ the value was only about 4 nm, which could be due to the significant reduction in particle size (Fig. 3i). It is seen from the topography that the aggregation was more in the case of NSZ55 than NSZ73, which led to an increase in  $R_a$  values (34 and 58 nm for NSZ-73 and NSZ-55 respectively). The difference in  $R_a$  value could possibly have an impact on the initial cell attachment. Hence, these coatings were further investigated to study the effect of surface topography on the initial adhesion behaviour of MG-63 osteoblast-like cells.

### 3.4 Adhesion Test

The adhesion tests were carried out for all the coatings NS, NZ, NSZ-73 and NSZ-55 according to ASTM standard. It is seen from the results that, NS coatings exhibited adhesion of 3B and small flakes of the coatings were detached along the edges and at intersections of cuts and the area affected is 5 to 15 % of the lattice. Whereas, NZ coatings exhibited adhesion of 4B and the detachment of the coatings at the intersections of the cuts was about 5%. These results confirming that NZ has relatively better adhesion compared to that of the NS coatings. NSZ-73 and NSZ-55 coatings also had adhesion of 4B respectively. Therefore, from the adhesion tests it is understood that the addition of Zr to NS coatings help to improve the adhesion of the coating to the substrate. The cross-sectional SEM morphology also further confirmed the same.

### 3.5 Surface wettability

Surface wettability of an implant material is also one of the

key aspects because it helps in improving the cell adhesion with implant.<sup>20</sup> The SBF contact angle (SBF-CA) values of uncoated and coated 316L SS samples were measured in static condition and the measured values are compared in Fig. 7. The contact angle value of NS was found to be less ( $\sim 39^\circ$ ) compared to NZ ( $\sim 130^\circ$ ) and uncoated 316L SS ( $\sim 95^\circ$ ). Three and two fold reductions in contact angle value of NS is caused by the existence of more hydrophilic group (-OH) on the surface. The increase in surface roughness value of NS compared to 316L SS, is also responsible for increased hydrophilicity of the coating. It has also been reported that the wettability increases with increasing surface roughness.<sup>33, 34</sup> The increase in SBF CA value for NZ coating could be attributed to the formation of relatively smooth surface, which possibly prevents the condensation of water droplets and considerably reduces the surface wettability.<sup>35</sup> The lower  $R_a$  value obtained for NZ coating from AFM line scanning is also in agreement with the above results. The contact angle values of NSZ-73 and NSZ-55 is  $\sim 45^\circ$  and  $\sim 55^\circ$  respectively. From the results it is seen that the contact angle values were significantly reduced for NSZ coating and slightly higher than that of NS. The above results indicated that the mixed oxide coatings also exhibited hydrophilic nature and the slight increase in contact angle value compared to NS could be attributed to the existence of micro/nano structure with compositional change of the surface.

### 3.6 Electrochemical corrosion behaviour

Fig. 8 shows the potentiodynamic polarization curves obtained for all the coated specimens in SBF solution. Uncoated 316 L SS is also included in the figure in order to show the efficiency of the coatings against corrosion. Polarization parameters viz., corrosion potential ( $E_{\text{corr}}$ ) and corrosion current density ( $i_{\text{corr}}$ ) values were derived from the obtained polarization curves and are compared in Fig. 9. It is noticed from the polarization curves that, the current densities of coated samples at cathodic and anodic regions are less compared to that of the uncoated 316L SS. These results indicating the reduced cathodic and anodic reaction rates of coated samples compared to that of the uncoated 316L SS. Furthermore, in the case of uncoated 316L SS, a sudden increase in current density was observed at about  $0.33 V_{\text{SCE}}$  and the same was not notable for the coated samples. This sudden increase in anodic current density is attributed to the breakdown of the passive film. The absence of this characteristic in the case of coated samples revealing the passive nature of the produced coatings. As can be seen from the results (Fig. 9) that, the uncoated samples exhibited corrosion current density ( $i_{\text{corr}}$ ) of about ( $0.8 \mu\text{A}/\text{cm}^2$ ) with corrosion potential ( $E_{\text{corr}}$ ) of  $-0.28 V_{\text{SCE}}$ . The obtained results are in good agreement with the available literature.<sup>36</sup> All the coated samples exhibited a significant reduction in  $i_{\text{corr}}$  and also shift in  $E_{\text{corr}}$  towards the positive potential confirming the improvement in corrosion resistance of the coatings. NS coatings exhibited about four times reduction in  $i_{\text{corr}}$  values with positive shift in  $E_{\text{corr}}$  of about  $0.25 V_{\text{SCE}}$  indicating the improved corrosion resistance. Whereas in the case of NZ, the  $i_{\text{corr}}$  values significantly reduced and is about 10 and three times lower than that of uncoated and NS respectively. In addition to that, the  $E_{\text{corr}}$  value also found to be  $0.13 V_{\text{SCE}}$

indicating the existence of thermodynamically stable coating. These results further confirming that NZ coatings could act as a barrier and effectively resist the penetration of aggressive Cl<sup>-</sup> ions into the coatings. It is interesting to note that the  $i_{\text{corr}}$  values of NSZ-73 (0.07  $\mu\text{A}/\text{cm}^2$ ) and NSZ-55 (0.05  $\mu\text{A}/\text{cm}^2$ ), are reduced than that of the NS and NZ. It is understood from the results that the addition of Zr to the NS coatings significantly alter the corrosion behavior. In particular, an increase in Zr content lead to the reduction of  $i_{\text{corr}}$  values, which is due to the formation of relatively compact coatings which could act as a barrier against the penetration of corrosive ions, which further confirmed from the surface and cross-sectional morphology of the coatings.

### 3.7 Cell attachment studies

Uncoated and coated 316L SS were evaluated for their initial cell attachment behaviour using MG 63 osteoblast-like cells. MG-63 osteoblast-like cell lines is one of the commonly used cell lines, which possess excellent interferon production material as well as growth capacity.<sup>37</sup> It is also used to study the cellular response of implant materials. MG-63 osteoblast-like cells were cultured on uncoated, NS, NZ, NSZ-73 and NSZ-55 coated 316L SS for 24 h. After 24 h, the cells were fixed with DAPI and actin to stain the cell nuclei and one of the cell protein components. It is relevant to the cytoskeleton organization which affects the cell substrate interaction and helps to study the initial cell attachment behaviour onto uncoated and coated samples. Fluorescence microscopic images of cell nuclei and actin were used to visualize the organization of MG 63 cell by fluorescence staining and are given in Fig. 10. At 24 h, MG-63 cells were found to be well adhered and spread throughout the surface of NS, NSZ-73, and NSZ-55. Over 316L SS and NZ, spherical morphology was seen for the cells, whereas in the case of NS, NSZ-73 and NSZ-55, the spherical morphology was gradually transformed into a well flattened morphology which confirmed the spreading nature of MG-63 cells. It is also reported that, SrO-SiO<sub>2</sub>-TiO<sub>2</sub> coatings enhance the cell attachment, spreading and proliferation rate.<sup>38</sup>

The organization of actin cytoskeleton over the surface is essential to control as well as to maintain the cell adhesion and shape. NS, NSZ-73 and NSZ-55 coatings induced the stress fibres composed of actin filaments over the surface. K. Marcy et al<sup>39</sup> have reported the higher proliferation rate of adipose-derived mesenchymal stem cell with proper fibroblast-like morphology for coatings compared to uncoated 316L SS. However, the actin cytoskeleton formation is not predominant in the case of NZ. The variation in cell attachment behaviour could possibly be explained by the surface chemistry and composition of the coatings. There are many factors involved in the control of cell adhesion over the implant surface and among them; surface wettability, surface charge and roughness are key factors. Increased hydrophilicity, and nano roughness were found to be suitable for cell adhesion whereas the cell adhesion were hindered over hydrophobic and smooth surface because, the existence of air layers between the substrate and medium led to the formation of 'virtual walls' that could hinder the direct contact between the surface and cells.<sup>40</sup> It is reported that the surface roughness in tens of nanometers are generally preferred by bone cells for adhesion, growth and differentiation more than

surface with sub-micron scale or even nanoscale roughness.<sup>41</sup> These results are in good agreement with the results obtained in the present investigation.

It is seen from the results that NS coating exhibited better actin stress fibre formation and could be due to its enhanced hydrophilic nature. Lipsika et al have also reported that silica nanoparticle (NP) coatings does not provide any adverse effect on the cell attachment of MC3T3 and also the cell proliferation rate increased as the culture period is increased.<sup>42</sup> The similar behaviour was also observed in the present work further confirms that the produced coatings are biocompatible. The presence of adsorbed water will be more in the case of NS due to its enhanced wettability which promotes the interface reaction between the surface and protein, subsequently favours the cellular response of NS coatings.<sup>43</sup> Cell adhesion and growth is beneficial on hydrophilic anatase TiO<sub>2</sub> than rutile TiO<sub>2</sub> which is relatively hydrophobic.<sup>44</sup> It is also important to understand that the cells are adhering on both the hydrophilic and hydrophobic surfaces. However, on the hydrophobic surfaces, constant contact is required between cell and substrate for cell division and proliferation.<sup>45</sup> NZ coating exhibited the spherical cell morphology and also the stress fibre formation is also not significant as in the case of NS, which could be attributed to the hydrophobic nature with smooth surface of the coating. In the case of NSZ-73 and NSZ-55 also the actin stress fibres were well identified around the spherical cell nuclei. The rearrangement of these actin fibre bundles produces the filopodia which further helps in physical linkage of nuclear matrix to the cytoskeleton via the nuclear lamins.<sup>19</sup> It is seen from the results that the surface characteristics viz., surface composition, surface roughness and wettability mainly contribute to the cell attachment behaviour over ceramic coatings.

## 4. Conclusions

The nano sized coatings viz., NS, NZ, NSZ-73 and NSZ-55 coatings were produced onto 316L SS by simple sol-gel technique at ambient temperature. The findings of the research are concluded as follows

1. The formation of SiO<sub>2</sub>, ZrO<sub>2</sub>, and SiO<sub>2</sub>-ZrO<sub>2</sub> were confirmed from the appearance of characteristic Si-O-Si<sub>str</sub>, Zr-O-Zr<sub>str</sub> and Si-O-Zr<sub>str</sub> peaks in ATR-IR spectra. Appearance of broad peak in XRD with peak shift towards higher 2 $\theta$  value also further substantiated the ATR-IR results and also revealed the presence of amorphous coatings.
2. SEM-EDAX results revealed the existence of distinct morphology with varying Zr content in the coating. NZ coating was found to be smooth compared to other coating and also the particle size was reduced and was confirmed from particle size analysis.
3. Adhesion test clearly indicated the better adhesion behaviour of the produced coatings. The  $R_a$  values of the coatings from AFM studies were found to increase with increasing Zr content revealing the aggregation of spherical particles.
4. Potentiodynamic polarization studies revealed that the coatings significantly improved the corrosion resistance in SBF solution. In particular the addition of Zr to NS coatings resulted in reduction of  $i_{\text{corr}}$  values and better corrosion resistance than NS, NZ and uncoated 316L SS.

5. MG 63 osteoblast-like cell attachment studies over the uncoated and coated samples depended on the surface roughness, composition and hydrophilic/hydrophobic nature. Cell attachment was better for NS compared to other coatings and uncoated sample due to its relatively better hydrophilicity. In the case of NZ the cell attachment was not significant and was attributed to the relatively low  $R_a$  and hydrophobic nature. Combination of NS and NZ with NSZ-73 and NSZ-55 showed remarkable difference in cell attachment and is not only related to  $R_a$  but also attributed to the surface chemical composition.

## Acknowledgements

The authors would like to acknowledge the financial assistance received from Department of Science and Technology-Science and Engineering Research Board (DST-SERB), Government of India, New Delhi to carry out this work (SR/S1/PC-14/2010 dt: 08.02.2011). Facilities provided by DST-FIST and UGC-DRS are also gratefully acknowledged.

## Notes

Department of Chemistry, College of Engineering Guindy Campus, Anna University, Chennai-600 025, Tamilnadu, INDIA.

\* Corresponding author

Email: nrAjendran@annauniv.edu

Tel: +91-44-22358659, Fax: +91-44-22200660.

## References

1. K. Kato, A. Yamamoto, S. Ochiai, M. Wada, Y. Daigo, K. Kita, K. Omori, *Mater. Sci. Eng. C*, 2013, **33**, 2736.
2. D. Rajeswari, D. Gopi, S. Ramya, L. Kavitha, *RSC Adv.*, 2014, **4**, 61525.
3. V. Quang Le, A. Cochis, L. Rimondini, G. Pourroy, V. Stanic, H. Palkowski, A. Carrado, *RSC Adv.*, 2013, **3**, 11255.
4. Karim Bordji, Jean-Yves Jouzeau, Didier Mainard, Elisabeth Payan, Jean-Pierre Delagoutte, Patrick Netter, *Biomaterials*, 1996, **17**, 491.
5. M. Talha, C. K. Behera, S. Kumar, Om Pal, G. Sing, O. P. Sinha, *RSC Adv.*, 2014, **4**, 13340.
6. U. Kamachi Mudali, T. M. Sridhar, Baldev Raj, *Sadhana*, 2003, **28** (3, 4), 601.
7. M. Talha, C. K. Behera, O. P. Sinha, *Mater. Sci. Eng. C*, 2013, **33**, 3563.
8. L. Cardenas, J. MacLeod, J. Lipton-Duffin, D. G. Seifu, F. Popescu, M. Sij, D. Mantovani, F. Rosei, *Nano Scale*, 2014, **6**, 8664.
9. A. Ochsenbein, F. Chai, S. Winter, M. Traisnel, J. Breme, H. F. Hildebrand, *Acta Biomater.*, 2008, **4**, 1506.
10. A. Duran, A. Conde, A. G. Coedo, T. Dorado, C. Garcia, S. Cere, *J. Mater. Chem.*, 2004, **14**, 2282.
11. S. R. Paital, N. B. Dahotre, *Mater. Sci. Eng. R*, 2009, **66**, 1.
12. S. Nagarajan, N. Rajendran, *Appl. Surf. Sci.*, 2009, **255**(7), 3927.
13. L. Cordero-Arias, S. Cabanas-Polo, H. Gao, J. Gilbert, E. Sanchez, J. A. Roethar, D. W. Schubert, S. Virtanen, A. R. Boccaccini, *RSC Adv.*, 2013, **3**, 11247.
14. S. Nagarajan, N. Rajendran, *Mater. Chem. Phys.*, 2010, **119** (3), 363.
15. S. Anne Pauline, U. Kamachi mudali, N. Rajendran, *Mater. Chem. Phys.*, 2013, **142** (1), 27.
16. M. F. Morks, A. Kobayashi, *J. Mech. Behav. Biomed. Mater.*, 2008, **1**, 165.
17. M. Mazrooei, M. H. Fathi, *Ceram. Int.*, 2012, **38**, 1325.
18. Dean-Mo Liu, Quanzu Yang, Tom Troczynski, *Biomaterials*, 2002, **23**, 691.
19. K. Anselme, *Biomaterials*, 2000, **21**, 667.
20. T. Ishizaki, N. Saito, O. Takai, *Langmuir*, 2010, **26**(11), 8147.
21. S. M. Hosseinalipour, A. Ershad-langroudi, Amir Nemati Hayati, A. M. Nabizade-Hanhighi, *Prog. Org. Coat.*, 2010, **67**, 371.
22. S. Nagarajan, P. Sudhagar, M. Mohana, V. Raman, T. Nishimura, Sanghyo Kim, Yong Soo Kang, N. Rajendran, *ACS Appl. Mater. Interfaces*, 2012, **4**(10), 5134.
23. D. O. Costa, P. D.H. Prowse, T. Chrones, S. M. Sims, D. W. Hamilton, A. S. Rizkalla, S. J. Dixon, *Biomaterials*, 2013, **34**(30), 7215.
24. T. Kokubo, H. Takadama, *Biomaterials*, 2006, **27**, 2907.
25. ASTM Designation: D 3359- 97 Standard Test Methods for Measuring Adhesion by Tape Test.
26. A. Srinivasan, P. Ranjany, N. Rajendran, *Electrochim. Acta*, 2013, **88**, 310.
27. Y. Zhang, L. Pan, C. Gao, Y. Wang, Y. Zhao, *J Sol-Gel Sci. Technol.*, 2010, **56**, 27.
28. J. Ch. Valmalette, M. Isa, *Chem. Mater.*, 2002, **14** (12), 5098.
29. J. M. E. Matos, F. M. Anjos Junior, L. S. Cavalcante, V. Santos, S. H. Leal, L. S. Santos Júnior, M. R. M. C. Santos, E. Longo, *Mater. Chem. Phys.*, 2009, **117**, 455.
30. N. R. Dhineshbabu, P. Manivasakan, R. Yuvakkumar, P. Prabu, V. Rajendran, *J Nanosci. Nanotechnol.*, 2013, **13**(6), 4017.
31. E. De Las Heras, D.A. Egidi, P. Corengia, D. González-Santamaría, A. Garcia-Luis, M. Brizuela, G.A. López, M. Flores Martinez, *Surf. Coat. Technol.*, 2008, **202**, 2945.
32. D. Buser, R. Schenk, S. Steinemann, J. Fiorellini, C. Fox, H. Stich, *J Biomed. Mater. Res.*, 1991, **25**, 889.
33. R. K. Iler, *John Wiley & Sons*, New York, 1979.
34. R. A. Fleming, Min Zou, *Appl. Surf. Sci.*, 2013, **280**, 820.
35. N. Michael, B. Bhushan, *Microelectron. Eng.*, 2013, **84**, 820.
36. G. Ramirez, S. E. Rodil, S. Muhl, D. T. Ortega, J. J. Olaya, M. Rivera, E. Camps, L. E. Alarcon, *J Non-Cryst. Solids* 2010, **356**, 2714.
37. A. Billiau, V. G. Edy, H. Heremans, J. Van Damme, J. Desmyter, J. A. Georgiades, P. Dr Somer, *Antimicrobial agents and chemotherapy*, 1977, **12**(1), 11.
38. C. Y. Zheng, F. L. Nie, Y. F. Zheng, Y. Cheng, S. C. Wei, L. Ruan, R. Z. Valiev, *Appl. Surf. Sci.*, 2011, **257**, 5913.
39. K. Marycz, J. Krzak, W. Urbanski, C. Pezowicz, *Journal of Nanomaterials*, Volume 2014, Article ID 350579.
40. Y. Wang, C. E. Sims, P. marc, M. Bachman, G. P. Li, N. L. Allbritton, *Langmuir*, 2006, **22** (19), 8257.
41. M. V. Drovcova, J. Hanus, M. Drabik, O. Kylian, H. Briederman, V. Lise, L. Bacakova, *J. Biomed. Mater. Res. Part A*, 2012, **100 A**, 1016-1032.
42. A. M. Lipski, C. J. Pino, F. R. Haselton, I. W. Chen, V. Prasad Shastri, *Biomaterials*, 2008, **29**, 3836.
43. G. Altankov, T. Groth, *J Mater. Sci. Mater. Med.*, 1994, **5**, 732.
44. J He, W. Zhou, X. Zhou, X. Zhang, P. Wan, B. Zhu, W. Chen, *J. Mater. Sci. Mater. Med.*, 2008, **19**, 3465.

45. A. K. Pannier, B. C. Anderson, L. D. Shea, *Acta Biomater.*, 2005, **1**, 511.

Table 2

## Table captions

**Table 1** Composition of sol used for the development of ceramic coatings.

**Table 2** Chemical composition of simulated body fluid (SBF) solution.

## Figure captions

**Fig. 1** ATR-IR spectra of ceramic coated 316L SS specimens.

**Fig. 2** XRD patterns of ceramic coated 316L SS specimens.

**Fig. 3** SEM images of (a, b) NS, (c, d) NZ, (e, f) NSZ-73 and (g, h) NSZ-55; (i) Average particle size and (j) EDAX chemical composition of coated samples.

**Fig. 4** Cross-sectional SEM surface morphologies of coated 316L SS.

**Fig. 5** AFM topographs, line scan patterns and histograms of (a) Uncoated, (b) NS, (c) NZ, (d) NSZ-73 and (e) NSZ-55.

**Fig. 6** Histogram of  $R_a$  roughness values of uncoated and coated 316L SS.

**Fig. 7** Simulated body fluid contact angle (SBF-CA) values of uncoated and coated 316L SS.

**Fig. 8** Potentiodynamic polarization curves of uncoated and coated 316L SS in SBF solution after 30 min. of exposure.

**Fig. 9** Comparison of potentiodynamic polarization parameters of uncoated and coated 316L SS.

**Fig. 10** DAPI and actin stained fluorescent images showing cell attachment (Merged images were obtained at 40X magnification).

Table 1

S. No	TEOS (ml)	Zr (IV) isopropoxide (ml)	EtOH (ml)	NaOH (g)	H <sub>2</sub> O (ml)	Sample code
1	1.20	0	10	0.01	6.0	NS
2	0	1.20	10	0.01	6.0	NZ
3	0.84	0.36	10	0.01	6.0	NSZ-73
4	0.60	0.60	10	0.01	6.0	NSZ-55

S. No	Reagents	Amount in 1000 ml
1	NaCl	8.035 g
2	NaHCO <sub>3</sub>	0.355 g
3	KCl	0.225 g
4	K <sub>2</sub> HPO <sub>4</sub> ·3H <sub>2</sub> O	0.231 g
5	MgCl <sub>2</sub> ·6H <sub>2</sub> O	0.311 g
6	1.0 M HCl	39.0 ml
7	CaCl <sub>2</sub>	0.292 g
8	Na <sub>2</sub> SO <sub>4</sub>	0.072 g
9	((HOCH <sub>2</sub> ) <sub>3</sub> CNH <sub>2</sub> )	6.118 g
10	1.0 M HCl	Appropriate amount for adjusting the pH ~ 7.4

Figure 1

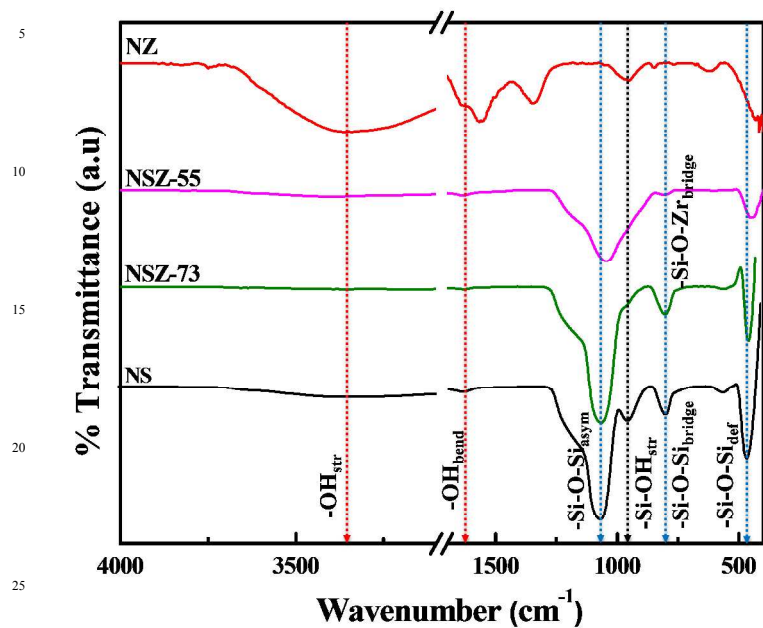


Figure 2

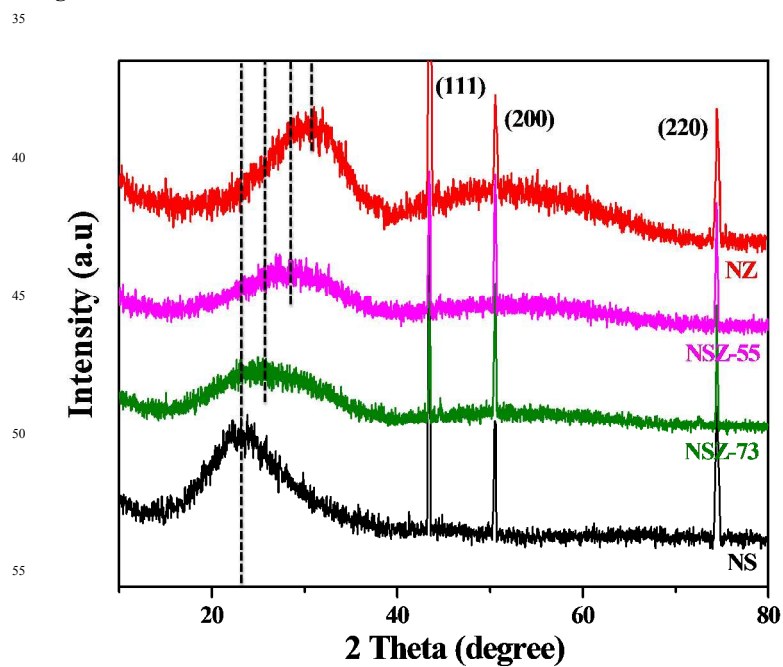
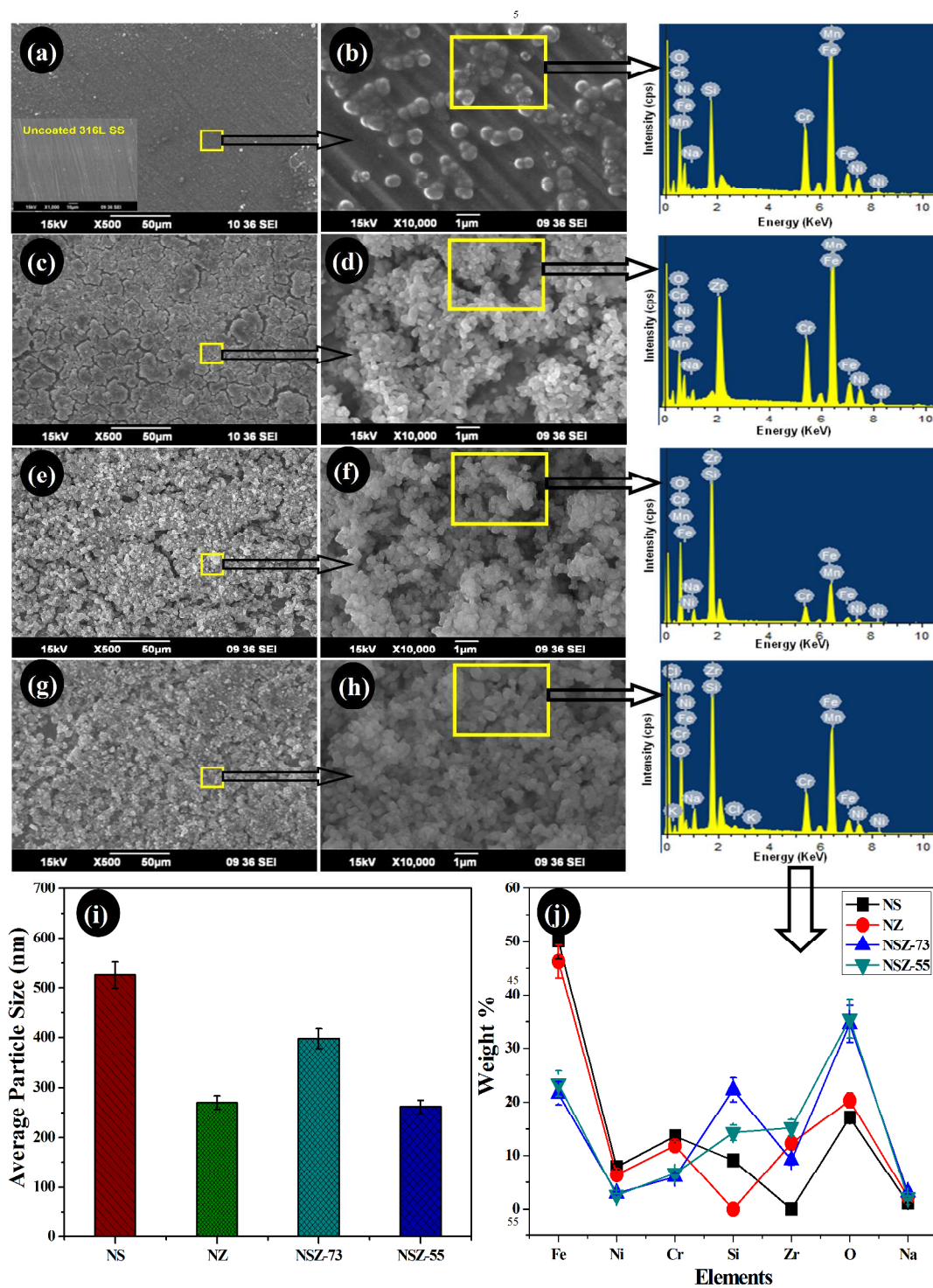


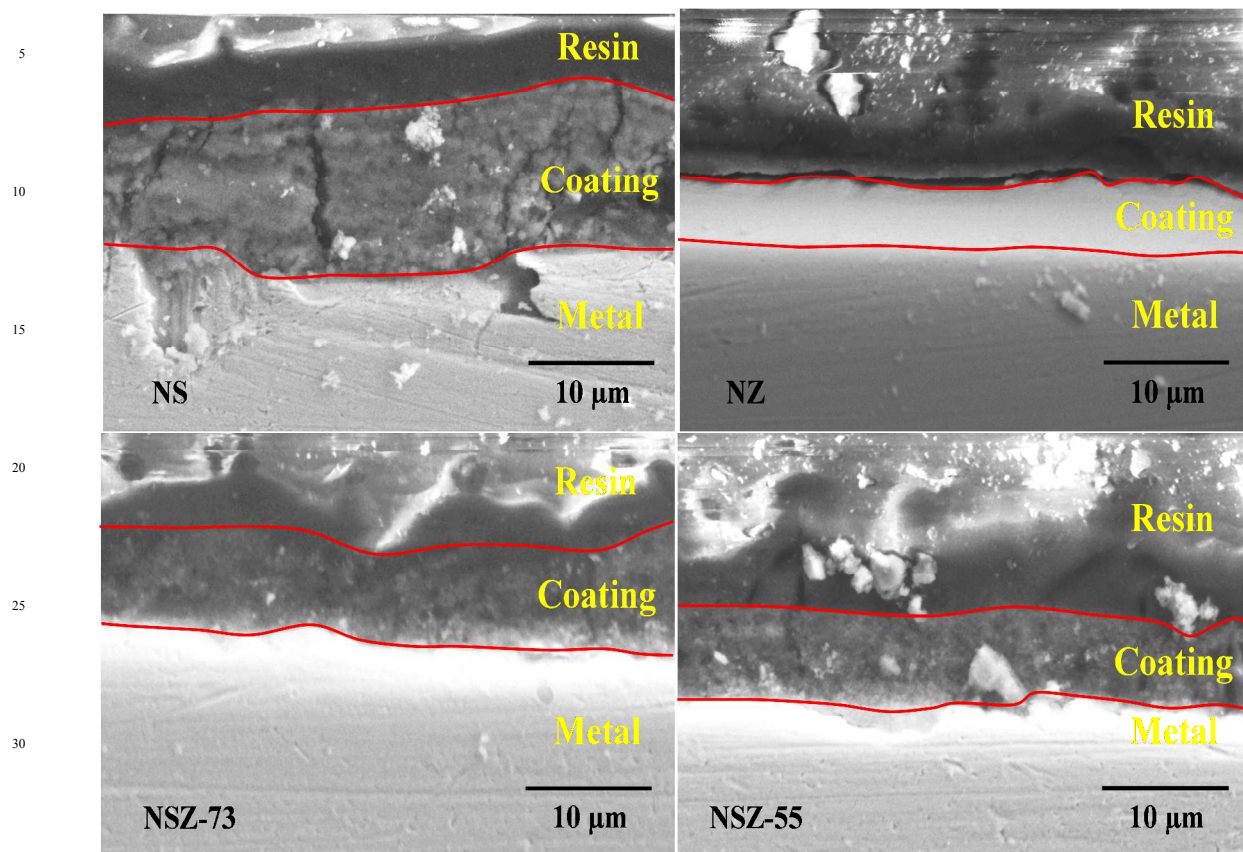
Figure 3



60

65

Figure 4



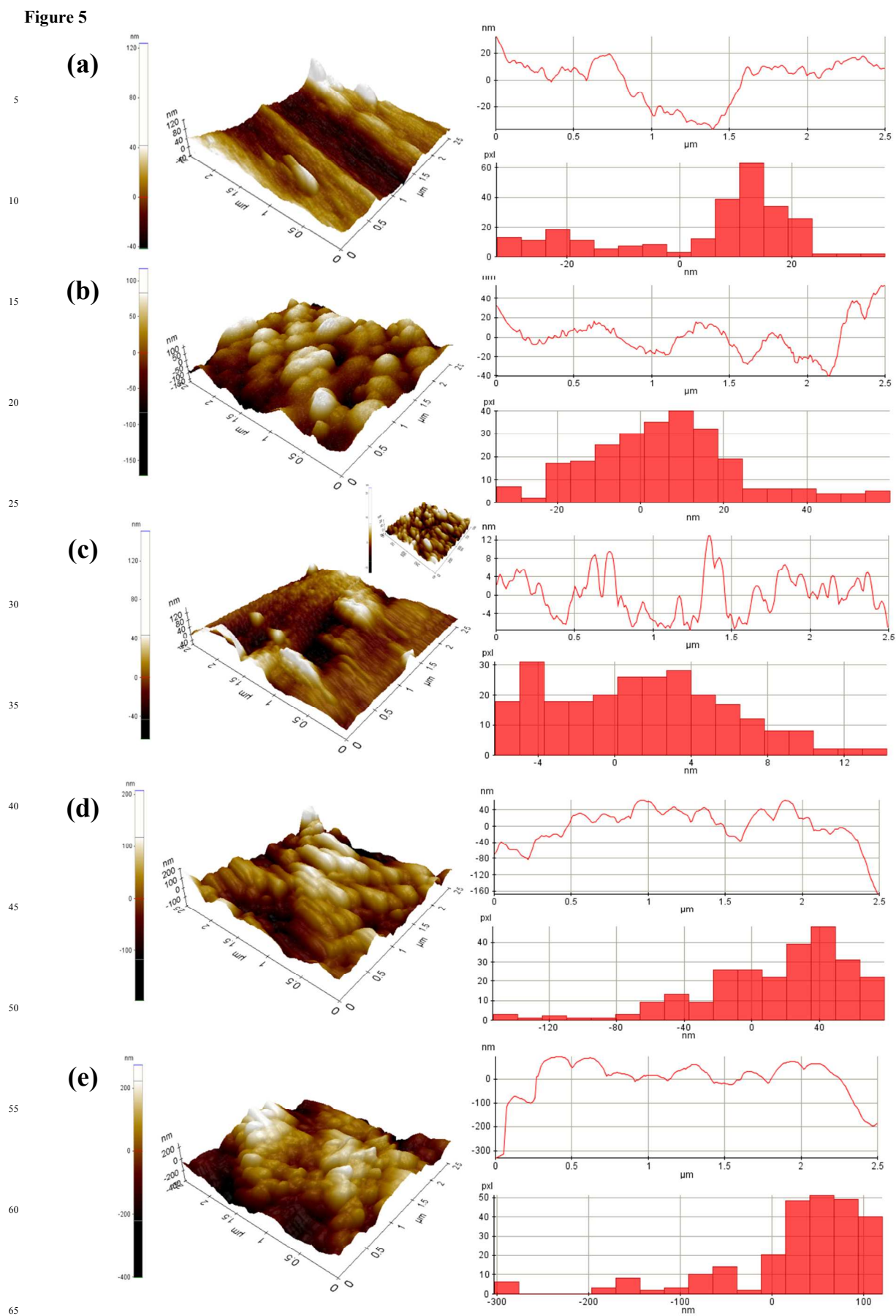


Figure 6

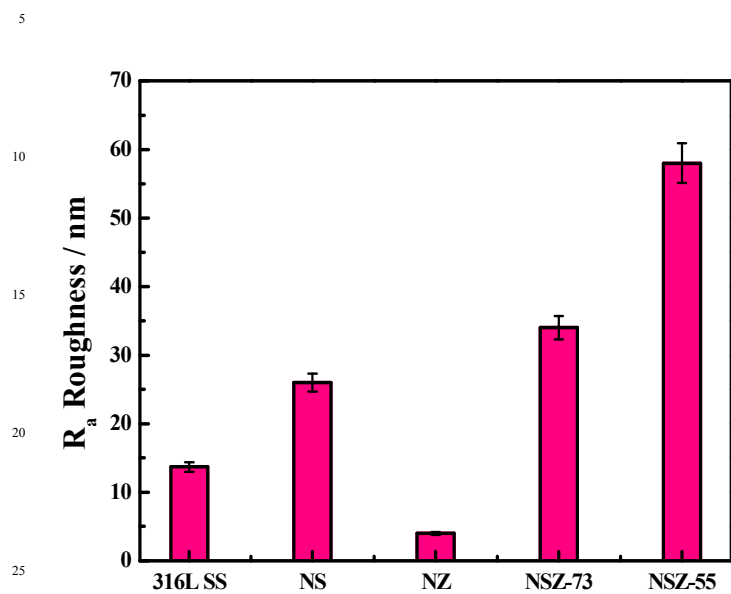


Figure 7

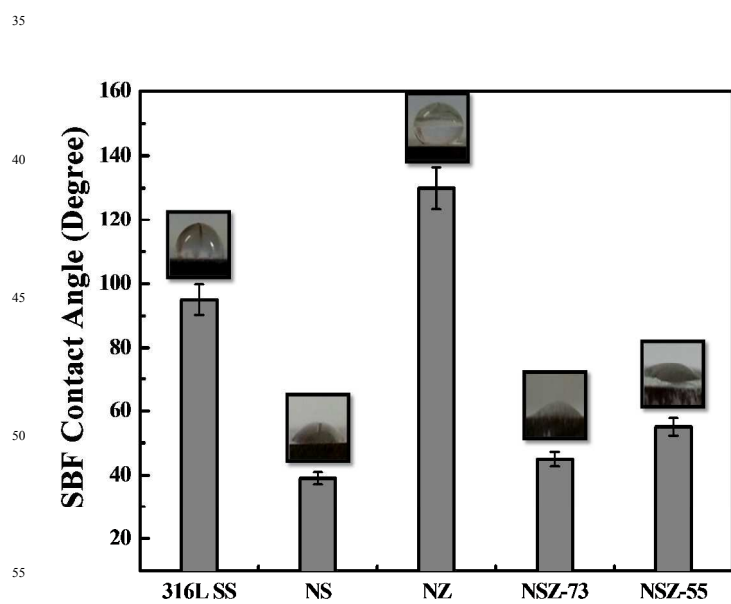


Figure 8

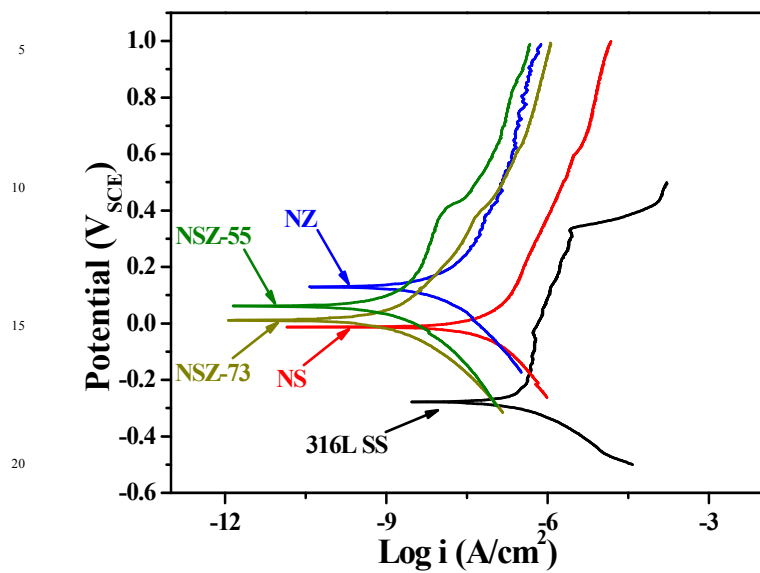
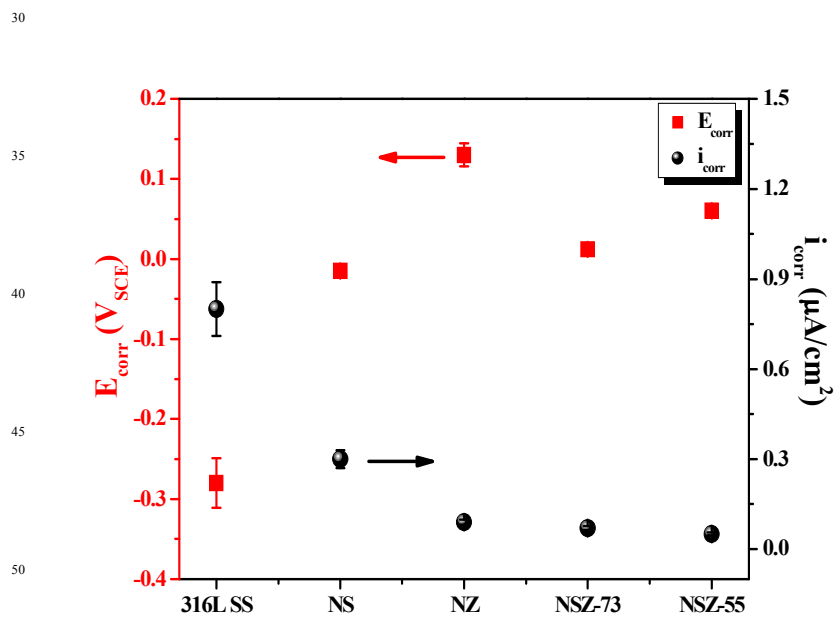
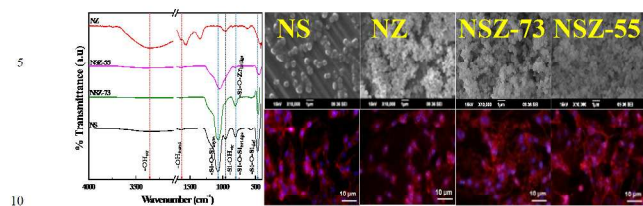


Figure 9





## TOC



Nano ceramic coatings were produced on to 316L SS. MG-63 Ostoblast like cells attachments were good for silica containing coatings.